Title: A novel ENU-induced ankyrin-1 mutation impairs parasite invasion and increases erythrocyte clearance during malaria infection in mice

Author list and affiliations

Hong Ming Huang[1], Denis C. Bauer[2], Patrick M. Lelliott[3], Andreas Greth[4], Brendan J. McMorran[1], Simon J. Foote[1], Gaetan Burgio[1]*

[1] Department of Immunology and Infectious Disease, John Curtin School of Medical Research, Australian National University, ACT, Australia.

[2] CSIRO, Sydney, NSW, Australia.

[3] IFReC Research Building, Osaka University, 3-1 Yamada-oka, Suita, Osaka 565-0871, Japan.

[4] synaps studios GmbH, Rebmoosweg 73A, CH-5200 Brugg, Switzerland.

Corresponding author*

Dr. Gaetan Burgio

The John Curtin School of Medical Research, Australian National University,

131 Garran Road, ACT 2601, Australia.

Gaetan.burgio@anu.edu.au

+61 2 612 59428

Abstract

Genetic defects in various red blood cell (RBC) cytoskeletal proteins have been long associated with changes in susceptibility towards malaria infection. In particular, while ankyrin (Ank-1) mutations account for approximately 50% of hereditary spherocytosis (HS) cases, an association with malaria is not well-established, and conflicting evidence has been reported. We describe a novel N-ethyl-N-nitrosourea (ENU)-induced ankyrin mutation MRI61689 that gives rise to two different ankyrin transcripts: one with an introduced splice acceptor site resulting a frameshift, the other with a skipped exon. *Ank-1*$^{(MRI61689/+)}$ mice exhibit an HS-like phenotype including reduction in mean corpuscular volume (MCV), increased osmotic fragility and reduced RBC deformability. They were also found to be resistant to rodent malaria *Plasmodium chabaudi* infection. Parasites in *Ank-1*$^{(MRI61689/+)}$ erythrocytes grew normally, but red cells showed resistance to merozoite invasion. Uninfected *Ank-1*$^{(MRI61689/+)}$ erythrocytes were also more likely to be cleared from circulation during infection; the "bystander effect". This increased clearance is a novel resistance mechanism which was not observed in previous ankyrin mouse models. We propose that this bystander effect is due to reduced deformability of *Ank-1*$^{(MRI61689/+)}$ erythrocytes. This paper highlights the complex roles ankyrin plays in mediating malaria resistance.

38 **Introduction**

39 Malaria is a mosquito-borne disease caused by the protozoan *Plasmodium*, responsible for many
40 deaths every year, mostly children [1]. In endemic regions with limited healthcare access, host
41 genetics is one of the major determinants of malaria susceptibility and survival [2-4]. This is evident
42 from the distributions of various genetic polymorphisms in humans, such as Duffy antigen negativity
43 and sickle cell trait, which coincide with malaria distribution [3,5,6]. It is thought that these genetic
44 polymorphisms confer protection against malaria, thus providing a survival advantage in the face of
45 malaria-induced mortality [7,8].

46 In addition, these polymorphisms also provide crucial insights into host-parasite interactions.
47 *Plasmodium* relies on a favourable host environment in order to thrive, many erythrocyte-related
48 polymorphisms have been discovered that interfere with parasite survival thus contributing to
49 malaria resistance. These include polymorphisms that affect the cytoskeleton of erythrocytes, such
50 as Southeast Asian Ovalocytosis (SAO), hereditary elliptocytosis (HE) and spherocytosis (HS) [9-13].
51 Several hypotheses have been proposed for the mechanisms by which they confer malaria
52 protection, including reduced erythrocyte invasion, intra-erythrocytic growth and cytoadherence [8,13-
53 19]. However, due to the heterogeneity of the manifestation of these disorders in the human
54 population, contradicting evidences for resistance mechanisms has often been presented. A study
55 done by Facer [13] showed that only patients carrying certain spectrin mutations have impaired
56 parasite invasion of red blood cells (RBC), but not others that also exhibited HE symptoms. A similar
57 observation was reported by Chishti, et al. [17], where individuals with defective protein 4.1 exhibited
58 intra-erythrocytic growth inhibition, but not those with glycophorin C defects, despite the fact that
59 both defects gave rise to HE. These differences in malaria resistance mechanisms remained largely
60 unexplored, and further studies in this aspect would potentially provide useful insight into host-
61 parasite interactions.

62 The RBC cytoskeletal protein ankyrin-1 (ANK-1), is a 210kDa protein responsible for connecting the
63 spectrin network with the RBC membrane through interactions with Band 3, protein 4.2 and the
64 Rhesus complex [20-22]. Spherocytosis is a genetic disorder where RBCs are abnormally small and are
65 known as spherocytes. ANK-1 mutations account for more than 50% of human HS cases [23]. However,
66 similar to SAO and HE, HS is a heterogeneous disorder where the symptoms vary greatly depending
67 on the mutations. The disorder can range from asymptomatic through to severe anaemia requiring
68 splenectomy [24]. Despite a possible association with malaria, HS is actually common in Northern
69 European and Japanese populations [25-28], and much rarer in other populations [29]. Nevertheless,
70 several *in vitro* and *in vivo* studies have repeatedly reported association between HS and malaria
71 resistance, and several mechanisms have been suggested. An *in vitro* study done by Schulman, et al.
72 [16] using RBCs from HS patients suggested that parasite invasion and growth in these erythrocytes
73 was impaired. This is further supported by studies done in mice with ankyrin mutations. Both *Ank-*
74 *1*$^{(nb/nb)}$ and *Ank-1* $^{(MRI23420/+)}$ have shown inhibited intra-erythrocytic growth and erythrocyte invasion
75 possibly due to spectrin and ankyrin deficiency, respectively [30,31]. On the other hand, another
76 mutation described by Rank, et al. [32], *Ank-1*$^{1674/+}$, parasite invasion appeared to be normal in these
77 erythrocytes. Instead, increased erythrocyte fragility was proposed as a contributing factor for
78 increased malaria resistance [32]. Taking these observations together, it is possible that disruption to
79 erythrocyte cytoskeletons can mediate multiple mechanisms of resistance.

80 In a large phenotypic N-ethyl-N-nitrosourea (ENU) mutagenesis screen, using either abnormal red
81 cells or resistance to malaria as to the screened phenotypes, we identified many novel mutations
82 that give rise to RBC abnormalities and consequently malaria resistance in mice. We report here an
83 ENU-induced mutation in the ankyrin-1 gene (*Ank-1*$^{(MRI61689)}$) which was found to exhibit a HS-like
84 phenotype, with significantly lower RBC volumes, increased osmotic fragility and decreased
85 deformability. *Ank-1*$^{(MRI61689)}$ also confers resistance towards *Plasmodium chabaudi adami* infection
86 in mice, and *Ank-1*$^{(MRI61689/+)}$ mice were shown to show both reduced merozoite invasion and
87 increased RBC clearance, possibly as a consequence of reduced red blood cell deformability.

88

89 **Results**

90 The MRI61689 mutation gives rise to an hereditary spherocytosis-like phenotype

91 The G1 mouse carrying the MRI61689 mutation was initially identified from an ENU suppressor
92 screen for the recessive mutation db/db. The G1 MRI61689 exhibited abnormal blood parameters on
93 an ADVIA haematological analyser, with reduced MCV of 48.6fL compared to the background of
94 53.3±0.5fL. This MCV values from the B6.BKS(D)-Lepr^{db}/J background is comparable to C57BL/6 mice.
95 We crossed the G1 founder mouse with B6.BKS(D)-Lepr^{db}/J to produce G2 mice where approximately
96 half of the animals exhibited an abnormal phenotype (Table 1). The affected G2 progeny, which
97 were obligate heterozygotes for the ENU-induced mutation, showed reduction in MCV (46.1±0.2fL)
98 compared to unaffected progeny (51.4±0.4fL), lower mean corpuscular haemoglobin (MCH)
99 (13.5±0.1pg compared to 14.6±0.1pg of wild-type), elevated RBC count (11.1±0.1x10^{9} cells/ml
100 compared to 10.5±0.1x10^{9} cells/ml of wild-type) (Table 1). No differences were observed for total
101 haemoglobin (HB), mean corpuscular haemoglobin concentration (MCHC), white blood cell (WBC)
102 count, platelets count (PLT) or reticulocyte percentage (Table 1).

103 However, when two affected mice were intercrossed, a quarter of the pups were found to die within
104 1 week postnatally, suggesting homozygosity for MRI61689 might be incompatible with life. Blood
105 smears were taken from these pups and compared with the other affected and unaffected mice. The
106 heterozygotes have slightly smaller RBCs but no target cells or spherocytes were observed (Figure
107 1a). Conversely, homozygous mice had significantly smaller RBCs with anisocytosis, fragmented RBCs,
108 acanthocytes and reticulocytosis (Figure 1a). Under SEM, RBCs of heterozygous mice seemed to have
109 less distinct discoid shape, but otherwise no distinguishing features were observed. (Figure 1b). On
110 the other hand, the RBCs of homozygous mice appeared very deformed, acanthocytic and appeared
111 to lack the discoid shape (Figure 1b).

112 When subjected to osmotic stress, RBCs of heterozygous mice showed significantly increased
113 fragility compared to wild-type erythrocytes (with 50% haemolysis at approximately 5.6 g/L
114 compared to 4.5 g/L of wild-type) (Figure 1c). The RBC deformability was assessed using an *in vitro*
115 spleen retention assay by filtering RBCs through a layer of beads with varying sizes. This is thought to
116 model splenic filtration *in vivo*, and the retention is thought to indicate deformability. As shown in
117 Figure 1d, the heterozygous mice exhibited up to 70% of the RBCs retention compared to wild-type
118 of approximately 3.5% retention, thus suggesting a significantly reduced RBC deformability.

119

120 MRI61689 carries a splice site mutation in *Ank-1* gene resulting in an alternative transcript and exon
121 skipping

122 To identify the causative mutation responsible for this abnormal RBC count, we sequenced the
123 exomes of 2 heterozygous mice. Exome sequencing revealed a number of variants. These were
124 prioritised based on filters as shown in Table 2. Through further genotyping using Sanger sequencing,
125 a mutation in *Ank-1* gene was found to correlate with all the affected mice and was proven to
126 segregate perfectly with the reduced MCV for over 3 generations of mouse crosses. The mutation
127 was found in the 17-18 intron of *Ank-1* gene, with T to A transversion 11 base pair upstream of exon
128 18 (IVS17-11T>A) (Figure 2a). This is situated in the ankyrin-repeats domain involved in band 3
129 binding. We proposed that the mutation introduced a new acceptor splice site for exon 18,
130 potentially leading to a frameshift mutation.

131 To assess this hypothesis, transcript analysis was performed. Embryonic liver RNA was extracted,
132 cDNA was synthesized and PCR-amplified using primers listed in the experimental procedures. Figure
133 2b shows the PCR products of embryonic liver cDNA from non-mutant, *Ank-1*$^{(MRI61689/+)}$ and *Ank-*
134 *1*$^{(MRI61689/MRI61689)}$ when amplified using primer set 1, which covers exon 17 to 21. Bands of
135 approximately 400bp can be observed in all the genotypes, but *Ank-1*$^{(MRI61689/MRI61689)}$ also exhibited a
136 second smaller product of approximately 300bp length. We proposed that this second band resulted

137 from exon skipping. Sanger sequencing of these PCR products revealed that the 300bp product
138 lacked exon 18, confirming that the exon 18 was skipped, and exon 19 was directly connected to
139 exon 17 during transcription (Figure 2c). This transcript is predicted to produce a shortened, in-
140 frame 207kDa ANK-1 protein.

141 To examine the effect of MRI61689 mutation in heterozygous mice, we further designed a primer set
142 containing the predicted acceptor splice site (primer set 2). Figure 2d shows that the mutant
143 transcript is only present in *Ank-1*$^{(MRI61689/+)}$ and *Ank-1*$^{(MRI61689/MRI61689)}$ mice, as predicted. Further
144 Sanger sequencing revealed an insertion of 11bp into the transcript adding an additional donor
145 splicing site and causing a frameshift mutation in the exon that would result in a premature stop
146 codon at amino acid position 724, as illustrated in Figure 2e, thus giving rise to a truncated protein of
147 78.5kDa. Therefore the homozygous mice exhibit a mutation at 11 bp upstream of the exon 18
148 donor splicing site resulting in two alternative transcripts: the skipping of exon 18 and an 11bp
149 insertion and creation of an additional donor splicing site leading to frameshift mutation that would
150 result in a premature stop codon and a truncated protein.

151 We hypothesize that this mutation would reduce the *Ank*-1 expression levels. We assessed this
152 hypothesis by examining the gene expression levels of *Ank-1* in embryonic liver using qPCR at mRNA
153 level and Western blotting at protein level in mature RBCs. As shown in Figure 3a, *Ank-1* mRNA
154 levels in both *Ank-1*$^{(MRI61689/+)}$ and *Ank-1*$^{(MRI61689/MRI61689)}$ E14 embryonic livers were significantly
155 reduced, up to 60% and 80% reduction compared to the wild-type, respectively. However, no
156 significant reduction in the full length ANK-1 (210kDa) protein levels was observed in both
157 Coomassie and Western blotting (Figure 3b-d). No truncated form of ANK-1 (78.5kDa) was observed
158 in *Ank-1*$^{(MRI61689/+)}$ erythrocytes. Furthermore, no reduction was observed for the protein levels of
159 other cytoskeletal proteins, including Band 3, protein 4.2, alpha- and beta-spectrin (Figure 3b and 3c).
160 This suggested that erythrocyte protein levels might be compensated by the WT allele in *Ank-*
161 *1*$^{(MRI61689/+)}$ mice, and the reduction in *Ank-1* mRNA levels did not seem to affect the protein levels.

162

163 *Ank-1*$^{(MRI61689/+)}$ mice are resistant to *Plasmodium chabaudi* infection

164 We hypothesized that the *Ank-1*$^{(MRI61689)}$ mutation confers malaria resistance. The malaria
165 susceptibility of *Ank-1*$^{(MRI61689/+)}$ mice was examined by injecting a lethal dose of *Plasmodium*
166 *chabaudi adami DS*, a murine strain of malaria that models the *Plasmodium falciparum* erythrocytic
167 stage [33]. The *Ank-1*$^{(MRI61689/+)}$ mice exhibited significantly lower peak parasitemia, with only
168 approximately 13% parasitemia compared to 52% parasitemia of wild-type (Figure 4a) but no delay
169 in the appearance of parasites was observed. In addition, *Ank-1*$^{(MRI61689/+)}$ have a significantly
170 increased survival rate, where all the *Ank-1*$^{(MRI61689/+)}$ mice survived the infection (Figure 4b)
171 compared to the 16% survival of wild-type mice. Since *Ank-1*$^{(MRI61689)}$ directly affects the red cell
172 (cytoskeletal protein), we hypothesized that the resistance was likely due to a RBC-autonomous
173 effect. Therefore, we postulated three mechanisms of *P. chabaudi* resistance in *Ank-1*$^{(MRI61689/+)}$ mice.
174 Firstly, the maturation of parasite inside the *Ank-1*$^{(MRI61689/+)}$ erythrocytes could be impaired leading
175 to reduced growth and death of parasites [31]. Secondly, the *Ank-1*$^{(MRI61689/+)}$ erythrocytes might be
176 resistant to merozoite invasion, which resulted in reduced parasitemia and delayed course of
177 infection [15]. Finally, the infected *Ank-1*$^{(MRI61689/+)}$ erythrocytes might more prone to destruction during
178 the course of infection (increased clearance), thus posing a challenge for the parasite to establish a
179 successful infection [34].

180

181 *Ank-1*$^{(MRI61689)}$ does not impair the intra-erythrocytic growth of *P. chabaudi*.

182 To elucidate the possible mechanisms of resistance, the effect of the *Ank-1*$^{(MRI61689/+)}$ mutation on
183 parasite intra-erythrocytic growth was investigated using the TUNEL assay at 1-10% parasitemia.
184 TUNEL detects DNA fragmentation, a marker for apoptosis or necrosis. In conjunction with a DNA
185 fluorescent dye, DAPI, it is possible to detect dying parasites in the erythrocytes (Figure 4c) [31,35]. We

186 measured the TUNEL-positivity of *P. chabaudi* in *Ank-1*$^{(MRI61689/+)}$ erythrocytes during the late
187 trophozoite stage of the infections, which was the portion of the parasite lifecycle affected by the
188 *Ank1* mutation in the *Ank-1*$^{(MRI23420/+)}$ line. As shown in Figure 4d, no differences was observed in the
189 percentage of TUNEL-positive parasites in both wild-type and *Ank-1*$^{(MRI61689/+)}$ erythrocytes (24.7 ± 2.3%
190 in *Ank-1*$^{(MRI61689/+)}$ mice compared to 29.5 ± 2.9% in wild-type). This indicated that *Ank-1*$^{(MRI61689)}$ did
191 not impair parasite intra-erythrocytic growth.

192

193 *Ank-1*$^{(MRI61689/+)}$ erythrocyte is resistant to *P. chabaudi* invasion, and have increased clearance from
194 circulation

195 Erythrocyte invasion and clearance were assessed via an *in vivo* erythrocyte tracking (IVET) assay.
196 Labelled blood of wild-type and *Ank-1*$^{(MRI61689/+)}$ mice were injected into infected wild-type mice
197 during merozoite invasion to examine the ability of *Plasmodium chabaudi* to invade and grow within
198 erythrocytes of both genotypes. The result compared the percentage of parasitized cells of both
199 genotypes and expressed as a ratio of parasitemia in *Ank-1*$^{(MRI61689/+)}$ RBC to wild-type RBC
200 populations. As shown in Figure 4e, lower parasitemia ratio (approximately 0.55) was observed from
201 30 minutes after injection with labelled blood, and was consistently lower in *Ank-1*$^{(MRI61689/+)}$ blood
202 over 36 hours post injection, which indicates a lower invasion rate into the *Ank-1*$^{(MRI61689/+)}$ RBCs.
203 Additionally, the remaining proportion of labelled RBCs was also monitored over the course of the
204 assay. A significant reduction of *Ank-1*$^{(MRI61689/+)}$ erythrocytes in infected mice compared to wild-type
205 erythrocytes was observed, with up to a 45% reduction in *Ank-1*$^{(MRI61689/+)}$ RBC number compared
206 with wild-type (Figure 4f). On the other hand, a smaller reduction was observed for *Ank-1*$^{(MRI61689/+)}$
207 erythrocytes compared to wild-type in uninfected mice, suggesting *Ank-1*$^{(MRI61689/+)}$ RBCs are more
208 likely to get cleared from circulation during malaria infection. As the percentage of infected
209 erythrocytes was low (5-20%) (Supp. figure 1), this indicates that the majority of the RBCs getting
210 cleared were uninfected RBCs, possibly as a result of bystander effect. This experiment suggested

211 that two possible mechanisms of resistance are both operating to produce the lower parasitemia
212 and increased survival in *Ank-1*$^{(MRI61689/+)}$ mice, the reduction of parasite invasion and increased
213 clearance of *Ank-1*$^{(MRI61689/+)}$ RBCs.

214

215 **Discussion**

216 We report a novel mutation in *Ank-1* gene, MRI61689, causing a hereditary spherocytosis-like
217 phenotype, with reduced MCV, increased osmotic fragility and reduced deformability. MRI61689 is
218 an intronic mutation between exon 17 and 18 where two possible splice variants could arise, one
219 has an introduced acceptor site resulting a frameshift, whereas the other consists of a skipped exon
220 18. The *Ank-1* mRNA levels were reduced, but no reduction in protein levels were observed. The
221 predicted truncated form (78.5kDa) was also not observed. *Ank-1*$^{(MRI61689/+)}$ mice also have increased
222 resistance to *Plasmodium chabaudi* infections, and the erythrocyte invasion was impaired but the
223 intra-erythrocytic growth appeared normal. The *Ank-1*$^{(MRI61689/+)}$ RBCs were also more likely to be
224 cleared from circulation during infection, an observation independent of number of parasitized
225 erythrocytes.

226 In comparison of *Ank-1*^{MRI61689} mice to other previously described *Ank-1* mouse models, they
227 appeared comparable to *Ank-1*^{MRI23420} mice, but more severe than *Ank-1*^{1674} and *Ank-1*^{nb} mice. More
228 specifically, most homozygous *Ank-1*$^{(MRI61689)}$ mice died within a week after birth, similar to
229 homozygous *Ank-1*^{MRI23420} mice, while homozygous *Ank-1*^{1674} and *Ank-1*^{nb} mice were viable [30,32].
230 However, no notable differences were observed in heterozygous *Ank-1*^{MRI61689} mice in terms of their
231 RBC microcytosis, morphology and susceptibility to osmotic stress compared to heterozygous *Ank-*
232 *1*^{1674} and *Ank-1*^{MRI23420} mice [31,32]. However, similar to *Ank-1*$^{1674/+}$ mice and unlike *Ank-1*$^{(MRI23420/+)}$ mice,
233 *Ank-1*$^{(MRI61689/+)}$ mice exhibited similar levels of ankyrin and other RBC cytoskeletal protein to wild-
234 type, which might suggest compensation by the wild-type allele, and thus warrants further studies.

235 In humans, many *ANK-1* mutations that result in frameshift have been described, most of which
236 situated in the band 3 binding domain towards the N terminus [36,37]. While no *Ank-1*$^{(MRI61689)}$
237 homologous mutation has been described in humans, a frameshift mutation has been reported to be
238 in the exon 17, called Ankyrin Osaka I, which gave rise to symptomatic HS [37]. Furthermore, exon
239 skipping in human *ANK-1* gene has also been documented. Edelman, et al. [38] reported a HS patient
240 exhibiting a severe ankyrin-deficient HS due to an introduction of a new splice acceptor site for exon
241 17, known as ankyrin^{Ankara}. Under further examination, this mutation was found to give rise to
242 multiple splice forms, including insertions and skipped exons. Most splice forms with insertion were
243 expected to cause frameshift, potentially leading to premature termination of ankyrin [38]. This finding
244 is in agreement with what we observed for *Ank-1*$^{(MRI61689/MRI61689)}$ mice, where frameshift caused by
245 new splice acceptor site, leading to high mortality rate with severe HS-like phenotype in *Ank-*
246 *1*$^{(MRI61689/MRI61689)}$ mice. It is likely that the surviving *Ank-1*$^{(MRI61689/MRI61689)}$ mice relied on the exon-
247 skipping splice form to produce in-frame functional *Ank-1* proteins. However, further studies are
248 required for support this hypothesis.

249 In terms of the response to malaria infection, *Ank-1*$^{(MRI61689/+)}$ mice exhibited similar degree of
250 malaria resistance as *Ank-1*$^{(MRI23420/+)}$ and *Ank-1*$^{1674/+}$ mice, with at least 30-40% reduction in
251 parasitemia and increased survival [31,32], and unlike *Ank-1*$^{nb/+}$ mice with only 10% reduction [30].
252 Previous studies suggested the reduction in erythrocyte invasion and intra-erythrocytic growth to be
253 the major resistance mechanisms [30,31]. However, normal parasite invasion was reported in *Ank-1*$^{1674/+}$
254 mice [32]. As a result, we have explored the potential mechanisms of *Ank-1*$^{MRI61689/+}$ mice in this study
255 in attempt to elucidate the complex roles ankyrin plays during malaria infections.

256 First, we report that *Ank-1*$^{(MRI61689/+)}$ mice exhibit normal parasite intra-erythrocytic growth (Figure
257 4d), in contrast to *Ank-1*$^{(MRI23420/+)}$ mice. TUNEL assay detects the presence of DNA fragmentation
258 which occurs during apoptosis and necrosis [39], which indicates dying parasites in RBCs [35]. McMorran,
259 et al. [35] reported TUNEL-positive parasites in C57BL/6 wild-type mice at a level consistent with the

260 observations in this study. On the other hand, Greth, et al. [31] reported a lower TUNEL-positive in
261 their SJL/J wild-type mice, which most likely due to differences in the genetic background of
262 experimental mice. Nevertheless, we did not observe abnormal parasite morphology under light
263 microscopy unlike *Ank-1*$^{(MRI23420/+)}$ mice, which support the deductions of parasite death from the
264 TUNEL assays.

265 In terms of parasite invasion, *Ank-1*$^{(MRI61689/+)}$ RBCs were found to be more resistant to merozoite
266 invasion as shown in the IVET assay (Figure 4e). The *Ank-1*$^{(MRI61689/+)}$ erythrocytes were less infected
267 compared to the wild-type 30 minutes after injection during merozoite invasion, and stayed
268 consistently lower compared to wild-type throughout the erythrocytic cycle. This reduction in
269 invasion has also been observed in *Ank-1*$^{(MRI23420/+)}$ mice [31]. In contrast, Rank, et al. [32] reported no
270 difference in parasite invasion for *Ank-1*$^{1674/+}$ mice, indicating a different effect mediated by *Ank-1*^{1674}
271 mutation compared to *Ank-1*$^{(MRI23420)}$ and *Ank-1*$^{(MRI61689)}$ mutations.

272 From these comparisons with other ankyrin mouse models, it is evident that RBC cytoskeleton plays
273 an important yet complex role during malaria infections. However the exact mechanism for each of
274 these different phenotypes for each ankyrin haplotype remains elusive, different ankyrin mutations
275 can exert different effects on the parasites depending on the location of the mutations, giving rise to
276 multiple resistance mechanisms. This hypothesis is also consistent with the heterogeneous HS
277 symptoms associated with ankyrin mutations, which highlights the complicated interactions
278 between RBC cytoskeletons and malaria parasites.

279 On the other hand, one important observation from the IVET assay is the rapid clearance of *Ank-*
280 *1*$^{(MRI61689/+)}$ erythrocytes from the circulation within 36 hours post-injection, up to 40% of the initial
281 RBC number (Figure 4f). However, at this timepoint the parasitemia of the host mice was only 5-20%
282 (Supp. Figure 1a), therefore the rate of RBC clearance cannot be explained by the clearance of
283 parasitized RBCs, instead, it is likely that the majority of the RBCs being cleared were uninfected. In
284 comparison, no loss was observed for wild-type erythrocytes in both infected and uninfected mice.

285 Since, in these experiments both wild-type and *Ank-1*$^{(MRI61689/+)}$ blood were subjected to the same
286 host environment simultaneously, it implies that the clearance of *Ank-1*$^{(MRI61689/+)}$ erythrocytes is cell
287 autonomous, rather than due to other effects of the host animal. This is the first observation of
288 increased, uninfected RBC clearance associated with an ankyrin mutation. Bystander clearance is
289 typically observed in inflammation, such as during sepsis [40], and is thought to cause severe malaria
290 anaemia during malaria infection in humans through the destruction of normal uninfected RBCs [41,42].
291 It is possible that *Ank-1*$^{(MRI61689)}$ causes a more exaggerated bystander effect during malaria infection,
292 leading to a rapid reduction of *Ank-1*$^{(MRI61689/+)}$ erythrocyte numbers.

293 Reduced RBC deformability was proposed to be one of the mechanisms of bystander clearance
294 during malaria anaemia through phagocytosis and splenic filtration [43,44]. From the *in vitro* spleen
295 retention assay (Figure 1d), *Ank-1*$^{(MRI61689/+)}$ erythrocytes exhibited reduced deformability, making
296 them more likely to be retained in the filter layer, which is likely to promote their destruction in *in*
297 *vivo* settings. Therefore, we proposed that *Ank-1*^{MRI61689} mutation causes alteration to the
298 erythrocyte, which renders them more likely to be cleared from the circulation.

299 In summary, we report that ENU-induced *Ank-1*^{MRI61689} mutation causes an HS-like phenotype in mice,
300 and confers significant resistance to *P. chabaudi* infection. We propose that *Ank-1*$^{(MRI61689/+)}$
301 erythrocytes are significantly resistant to parasite invasion but are able to support normal parasite
302 intra-erythrocytic growth. We also described a novel observation of increased RBC clearance
303 associated with this ankyrin mutation. This study emphasizes the importance of RBC cytoskeletal
304 proteins in mediating multiple complex mechanisms of resistance towards malaria, which provide
305 further insights to the complex interaction between the host and parasites.

306

307 **Methods and Materials**

308 Mice and Ethics Statement

309 All mice used in this study were housed with 12 hour light-dark cycle under constant temperature at
310 21 °C. All procedures were conformed to the National Health and Medical Research Council (NHMRC)
311 Australian code of practice. Experiments were performed under ethics agreement AEEC A2014/54,
312 which were approved by the Australian National University animal ethics committees.

313

314 ENU Mutagenesis and Dominant Phenotype Screening

315 B6.BKS(D)-Lepr^{db}/J male mice were injected intraperitoneally with two dose of 100 mg/kg ENU
316 (Sigma-Aldrich, St Louis, MO) at one week interval for a recessive suppressor screen of db/db
317 mutation. The treated males (G0) were crossed to females from the isogenic background to produce
318 the first generation progeny (G1). The seven-week-old G1 progeny were bled and analysed on an
319 Advia 120 Automated Haematology Analyser (Siemens, Berlin, Germany) to identify abnormal red
320 blood cell count. Mouse carrying MRI61689 mutation was identified with a "mean corpuscular
321 volume" (MCV) value three standard deviations lower from other G1 progeny. It was crossed with
322 B6.BKS(D)-Lepr^{db}/J mice to produce G2 progeny to test the heritability of the mutations and the
323 dominance mode of inheritance. Mice that exhibited low MCV (<48fL) were selected for whole
324 exome sequencing and genotyping. This abnormal red blood cell count was unrelated to the obesity
325 phenotype.

326

327 Microscopy

328 For light microscopy, cells were briefly fixed in methanol for one minute and air-dried before being
329 stained in a 10% Giemsa solution (Sigma-Aldrich, St Louis, MO) at pH 7.4 for 10 minutes. For
330 scanning electron microscopy (SEM), fresh blood was first fixed immediately upon drawing in 3%
331 EM-grade glutaraldehyde (Sigma-Aldrich, St Louis, MO) overnight at 4°C. The samples were washed
332 with mouse tonicity phosphate buffered saline (MT-PBS) (150mM NaCl, 16mM Na_2HPO_4, 4mM

333 NaH_2PO_4, pH 7.4) 3 times, 10 minutes soak each. The cells were then adhered to the cover slips with
334 0.1% polyethyleneimine (PEI) for 10 minutes, before washing off with MT-PBS. The cells were then
335 dried serially using 30%, 50%, 70%, 80%, 90%, 100%, 100% ethanol, each with 10 minutes soak. The
336 cells were then soaked in 1:1 ethanol: hexamethyldisilazane solution for 10 minutes, followed by 2
337 washes with 100% hexamethyldisilazane, each 10 minutes. The coverslips were then air-dried
338 overnight and coated with gold and examined under JEOL JSM-6480LV scanning electron microscope.

339

340 Osmotic Fragility Measurement

341 To assess the susceptibility of RBC membrane to osmotic stress, 5µl of mouse whole blood was
342 diluted 100-fold with phosphate buffer (pH 7.4) containing 0 to 10g/L of sodium, and incubated for
343 at least 10 minutes at room temperature. The cells were centrifuged at 800g for 3 minutes, and the
344 supernatant, which contains free haemoglobin, was measured at 540nm to assess the degree of
345 haemolysis. The absorbance values were expressed as percentage of haemolysis, with haemolysis at
346 0g/L sodium considered as 100% lysis.

347

348 *In vitro* spleen retention assay

349 The RBC deformability of both wild-type and *Ank-1*$^{(MRI61689/+)}$ were assessed according to the protocol
350 described previous by Deplaine, et al. [45] with modifications. Briefly, RBCs from wild-type and *Ank-*
351 *1*$^{(MRI61689/+)}$ mice were stained with 10µg/ml of either hydroxysulfosuccinimide Atto 633 (Atto 633) or
352 hydroxysulfosuccinimide Atto 565 (Atto 565) (Sigma-Aldrich, St Louis, MO), followed by three
353 washes with in MTRC (154mM NaCl, 5.6mM KCl, 1mM $MgCl_2$, 2.2mM $CaCl_2$, 20mM HEPES, 10mM
354 glucose, 4mM EDTA, 0.5% BSA, pH 7.4, filter sterilized). The stained RBCs were mixed in equal
355 proportion and diluted with unstained wild-type RBCs to give approximately 10-20% of the sample
356 being labelled RBCs. The samples were further diluted to 1-2% haematocrit with MTRC, before

357 passing through spleen retention filter bed. The pre-filtered and post-filtered samples were analysed
358 on BD LSRFortessa (BD Biosciences, Franklin Lakes, NJ) flow cytometer to determine the proportion
359 being retained in the filter bed.

360

361 Whole exome sequencing

362 DNA from two G2 mice carrying the abnormal red blood cell parameters (MCV <48fL) were extracted
363 with Qiagen DNeasy blood and tissue kit (Qiagen, Venlo, Netherlands) for exome sequencing as
364 previous described [46]. Briefly, at least 10µg of DNA was prepared for exome enrichment with Agilent
365 Sure select kit paired-end genomic library from Illumina (San Diego, CA), followed by high
366 throughput sequencing using a HiSeq 2000 platform. The bioinformatics analysis was conducted
367 according to the variant filtering method previously described by Bauer, et al. [47]. Private variants
368 that were shared between the two mutants but not with other B6.BKS(D)-Lepr^{db}/J, C57BL/6 mice or
369 previously described ENU mutants were annotated using ANNOVAR [48]. Private non-synonymous
370 exonic and intronic variants within 20 bp from the exon spicing sites were retained as potential
371 candidate ENU mutations.

372

373 PCR and Sanger sequencing

374 DNA from mutant mice were amplified through PCR with 35 cycles of 30 seconds of 95^{0}C
375 denaturation, 30 seconds of 56-58^{0}C annealing and 72^{0}C elongation for 40 seconds. The primers
376 used in the PCR are described as below. The PCR products were examined with agarose gel
377 electrophoresis before being sent to the Australian Genome Research Facility (AGRF) in Melbourne,
378 Australia, for Sanger sequencing. Logarithm of odds (LOD) score was calculated based on the
379 number of mice that segregated with the candidate mutations.

380 Primers:

381 *Acp5*-F: 5'-CAGAAGGATGCCTTTGGGTA-3'; *Acp5*-R: 5'-ACCAGCGCTTGGAGATCTTA-3'

382 *Kcnk1*-F: 5'-GGGCCTTTTCCTCCTTACAGA-3'; *Kcnk1*-R: 5'-CAGGAAACGGTGACAAATCC-3'

383 *Epas1*-F: 5'-GGAAGCCAGAACTTCGATGA-3'; *Epas1*-R: 5'-GTAGTGTTCCCTGGGGTGT-3'

384 *Picalm*-F: 5'-TCACTGAATGTAATTGGGATATCAT-3'; *Picalm*-R: 5'-CACCCTCTCTTCACTTTTGTG-3'

385 *Socs6*-F: 5'-CCGCTTTGTTATCCGTCAGT-3'; *Socs6*-R: 5'-TGGCAGCAAAGACTTCAATG-3'

386 *Ank1*-F: 5'-TCCCTGGCTTAAAGTTGGTG-3'; *Ank1*-R: 5'-CTCTCCCTTAGCTGCATTCC-3'

387

388 Quantitative PCR and cDNA sequencing

389 RNA was isolated from embryonic livers of E14 embryos using Qiagen RNeasy kit (Qiagen, Venlo,
390 Netherlands), followed by cDNA synthesis using Transcriptor High Fidelity cDNA Synthesis Kit (Roche,
391 Basel, Switzerland). Quantitative PCR was carried out on ViiA™ 7 Real-Time PCR System (Thermo
392 Scientific, Waltham, MA). The $\Delta\Delta C_T$ method [49] was used to determine the cDNA levels of *Ank-1* and
393 the housekeeping gene β-actin and expressed as a fold-change of the mutants to the wild-type. The
394 primers used for *Ank-1* gene spanned exon 2 to 4: *Ank-1*-F: 5'-TAACCAGAACGGGTTGAACG-3'; *Ank-1*-
395 R: 5'-TGTTCCCCTTCTTGGTTGTC-3'; β-Actin-F: 5'- TTCTTTGCAGCTCCTTCGTTGCCG-3'; β-Actin-R: 5'-
396 TGGATGCGTACGTACATGGCTGGG-3'.

397 To characterize the effect of MRI61689 mutation, cDNA were amplified through PCR using two
398 primers set were design as shown below: Primer set 1 was designed to amplify wild-type *Ank-1*
399 transcript, whereas primer set 2 was designed to only amplify the predicted mutant transcript with
400 11bp insertion. Amplified PCR product were analysed using agarose gel electrophoresis and each
401 band was purified and sequenced.

402 Primer set 1: Forward: ATGCAGAGTCGGTACAAGGC; Reverse: CCGTTCGAGCTGACCTCATT

403 Primer set 2: Forward: CCTGGGGAACAAGTTTCTTT; Reverse: GTGCAAGGGGCTGTATCCTA

404

405 SDS-PAGE, Coomassie staining and Western blot

406 RBC ghosts were prepared by lysing mouse RBCs with ice-cold 5mM phosphate buffer (ph7.4) and
407 centrifuged at 20,000g for 20 minutes followed by removal of the supernatant. The pellet was
408 further washed with the 5mM phosphate buffer until the supernatant became clear. The RBC ghosts
409 or whole blood lysates were denatured in SDS-PAGE loading buffer (0.0625M Tris pH 6.8, 2% SDS, 10%
410 glycerol, 0.1M DTT, 0.01% bromophenol blue) at 95°C for 5 minutes before loading onto a Mini-
411 PROTEAN® TGX™ Precast Gels (Bio-Rad, Hercules, CA). The gels were then either stained with
412 Coomassie blue solution (45% v/v methanol, 7% v/v acetic acid, 0.25% w/v Brilliant Blue G) overnight
413 or transferred to a nitrocellulose membrane. The western blot was carried out using these primary
414 antibodies: anti-alpha 1 spectrin (clone 17C7), anti-beta 1 spectrin (clone 4C3) (Abcam, Cambridge,
415 UK), anti-GAPDH (clone 6C5) (Merck Millipore, Darmstadt, Germany), anti-N-terminal *Ank-1* "p89",
416 anti-Band 3 and anti-protein 4.2 (kind gifts from Connie Birkenmeier, Jackson Laboratory, US).

417

418 Malaria infection

419 250µl of thawed *P. chabaudi adami* infected blood was injected into the intraperitoneal cavity of a
420 C57BL/6 donor mouse. When the donor mouse reached 1-10% parasite load (parasitemia), blood
421 was collected through cardiac puncture. The parasitized blood was diluted with Krebs' buffered
422 saline with 0.2% glucose as described previously [50]. Each experimental mouse was infected with
423 $1x10^4$ parasites intraperitoneally. The parasitemia of these mice were monitored either using light
424 microscopy or flow cytometry.

425

426 Terminal deoxynucleotidyl transferase dUTP nick end labelling (TUNEL) staining

427 3µl of infected blood containing 1-10% parasitemia were collected during trophozoite stage and
428 fixed in 1 in 4 diluted BD Cytofix™ Fixation Buffer (BD Biosciences, Franklin Lakes, NJ) for at least day
429 until they were needed. Each sample was then washed twice with MT-PBS, and adhered to a glass
430 slide pre-coated with 0.1% polyethylenimine (PEI) for 10 minutes at room temperature. The excess
431 cells were washed off with the wash solution from APO-BrdU TUNEL assay kit (Thermo Scientific,
432 Waltham, MA) and incubated overnight at room temperature with TUNEL labelling solution (1mM
433 Cobalt Chloride, 25mM Tris-HCl pH 6.6, 200mM sodium cacodylate, 0.25mg/ml BSA, 60uM BrdUTP,
434 15U Terminal transferase). The slides were washed three times with rinse buffer from APO-BrdU
435 TUNEL assay kit, followed by staining with 50µg/ml of anti-BrdU-Biotin antibody (Novus Biologicals,
436 Littleton, CO) in MT-PBT (MT-PBS, 0.5% BSA, 0.05% Triton X-100) for 1 hour. The slides were then
437 washed three times with MT-PBT, followed by probing with 2µg/ml Alexa Fluor® 594 conjugated
438 streptavidin (Thermo Scientific, Waltham, MA). Next, they were washed three times with MT-PBS
439 and mounted with SlowFade® Gold antifade reagent with DAPI (Thermo Scientific, Waltham, MA)
440 and sealed. When the slides were dried, they were examined using Axioplan 2 fluorescence light
441 microscope (Carl Zeiss, Oberkochen, Germany) between 600x to 1000x magnification. At least 100
442 DAPI-positive cells were counted, and each was graded as either positive or negative for TUNEL
443 staining, as an indication of DNA fragmentation.

444

445 *In vivo* erythrocyte tracking (IVET) assays

446 The IVET assay was carried out as previously described by Lelliott, et al. [51,52]. Briefly, 1.5ml to 2ml of
447 whole blood was collected from wild-type and *Ank-1*$^{(MRI61689/+)}$ mice via cardiac puncture. Both wild-
448 type and *Ank-1*$^{(MRI61689/+)}$ blood were either stained with 10µg/ml of Atto 633 or 125µg/ml of EZ-
449 Link™ Sulfo-NHS-LC-Biotin (Biotin) (Thermo Scientific, Waltham, MA) for 45 minutes at room
450 temperature, followed by washing three times with MT-PBS. The *Ank-1*$^{(MRI61689/+)}$ blood was mixed
451 with wild-type blood in two different dye combinations to correct for any dye effects. $1x10^9$

452 erythrocytes were injected intravenously into infected wild-type mice at 1-5% parasitemia during
453 schizogony stage, usually 8-10 days post-infection with $1x10^4$ parasites. Blood samples were
454 collected at 30 minutes, 3hours, 12 hours, 20 hours and 36 hours after injection. The ratio of
455 infected *Ank-1*$^{(MRI61689/+)}$ to wild-type erythrocytes was determined on flow cytometry, as an
456 indication of the relative susceptibility to malaria infections between wild-type and *Ank-1*$^{(MRI61689/+)}$
457 mice. The proportion of labelled blood populations were also tracked over time to determine the
458 clearance of these RBCs from the circulation.

459

460 Flow cytometry analysis of blood samples

461 For both malaria infections and IVET assay, 2µl of whole blood samples were stained with 2µg/ml
462 streptavidin-PE-Cy7 (only for experiments with biotinylated erythrocytes), 1µg/ml anti-CD45–
463 allophycocyanin (APC)–eFluor 780 (clone 30-F11), 1µg/ml anti-CD71 (TFR1)–PerCP–eFluor 710 (clone
464 R17217) (eBioscience, San Diego, CA), 4µM Hoechst 33342 (Sigma-Aldrich, St Louis, MO) and 12µM
465 JC-1 (Thermo Scientific, Waltham, MA) in MTRC. All samples analysed through flow cytometry were
466 performed on BD LSRFortessa (BD Biosciences, Franklin Lakes, NJ), where 100,000 to 2,000,000
467 events were collected and visualized on FACSDiva™ and FlowJo software. The RBCs and leukocytes
468 were first selected on forward scatter and side scatter channels (FSC/SSC) signals, followed by gating
469 of single cells based on FS area to height ratio. RBCs were further isolated by gating on CD71
470 negative and CD45 negative population, followed by gating on Atto-labelled and Biotin-labelled
471 erythrocytes on appropriate channels (APC for Atto-633, PE for Atto-565 and PE-Cy7 for Biotin). The
472 parasitemia of each labelled erythrocyte population was determined by gating on Hoechst 33342
473 positive and JC-1 positive population.

474

475 Statistical analysis

476 The LOD score method coupled with Bonferroni correction was used to determine the causative
477 mutation for MRI61689. The statistical significance of the malaria survival was tested using the Log-
478 Rank test. The statistical significance of parasite infection was determined via the statmod software
479 package for R (http://bioinf.wehi.edu.au/software/compareCurves) using the
480 'compareGrowthCurves' function with 10,000 permutation, followed by adjustments for multiple
481 testing. The statistical significance for the ratios of IVET assays was determined using the one sample
482 t-test with hypothetical mean of 1. For the rest of the results, statistical significance was determined
483 using two-tailed Students t-tests.

484

485 **References**

486 1 W.H.O. *World Malaria Report 2015*. (World Health Organisation (WHO), 2015).
487 2 Kwiatkowski, D. P. How malaria has affected the human genome and what human genetics
488 can teach us about malaria. *Am J Hum Genet* **77**, 171-192 (2005).
489 3 Piel, F. B. *et al.* Global distribution of the sickle cell gene and geographical confirmation of
490 the malaria hypothesis. *Nature communications* **1**, 104, doi:10.1038/ncomms1104 (2010).
491 4 Carter, R. & Mendis, K. N. Evolutionary and historical aspects of the burden of malaria. *Clin*
492 *Microbiol Rev* **15**, 564-594 (2002).
493 5 Zimmerman, P. A. *et al.* Emergence of FY*A(null) in a Plasmodium vivax-endemic region of
494 Papua New Guinea. *Proc Natl Acad Sci U S A* **96**, 13973-13977 (1999).
495 6 Miller , L. H., Mason , S. J., Clyde , D. F. & McGinniss , M. H. The Resistance Factor to
496 Plasmodium vivax in Blacks. *New England Journal of Medicine* **295**, 302-304,
497 doi:doi:10.1056/NEJM197608052950602 (1976).
498 7 Cyrklaff, M. *et al.* Hemoglobins S and C interfere with actin remodeling in Plasmodium
499 falciparum-infected erythrocytes. *Science* **334**, 1283-1286, doi:10.1126/science.1213775
500 (2011).
501 8 Allen, S. J. *et al.* Prevention of cerebral malaria in children in Papua New Guinea by
502 southeast Asian ovalocytosis band 3. *Am J Trop Med Hyg* **60**, 1056-1060 (1999).
503 9 Jarolim, P. *et al.* Deletion in erythrocyte band 3 gene in malaria-resistant Southeast Asian
504 ovalocytosis. *Proceedings of the National Academy of Sciences of the United States of*
505 *America* **88**, 11022-11026 (1991).
506 10 Mgone, C. S. *et al.* Occurrence of the erythrocyte band 3 (AE1) gene deletion in relation to
507 malaria endemicity in Papua New Guinea. *Trans R Soc Trop Med Hyg* **90**, 228-231 (1996).
508 11 Genton, B. *et al.* Ovalocytosis and cerebral malaria. *Nature* **378**, 564-565,
509 doi:10.1038/378564a0 [doi] (1995).
510 12 Lecomte, M. C. *et al.* [Hereditary elliptocytosis in West Africa: frequency and repartition of
511 spectrin variants]. *C R Acad Sci III* **306**, 43-46 (1988).
512 13 Facer, C. A. Erythrocytes carrying mutations in spectrin and protein 4.1 show differing
513 sensitivities to invasion by Plasmodium falciparum. *Parasitol Res* **81**, 52-57 (1995).

14 Kidson, C., Lamont, G., Saul, A. & Nurse, G. T. Ovalocytic erythrocytes from Melanesians are resistant to invasion by malaria parasites in culture. *Proceedings of the National Academy of Sciences of the United States of America* **78**, 5829-5832 (1981).

15 Hadley, T. *et al.* Resistance of Melanesian elliptocytes (ovalocytes) to invasion by Plasmodium knowlesi and Plasmodium falciparum malaria parasites in vitro. *J Clin Invest* **71**, 780-782 (1983).

16 Schulman, S. *et al.* Growth of Plasmodium falciparum in human erythrocytes containing abnormal membrane proteins. *Proc Natl Acad Sci U S A* **87**, 7339-7343 (1990).

17 Chishti, A. H., Palek, J., Fisher, D., Maalouf, G. J. & Liu, S. C. Reduced invasion and growth of Plasmodium falciparum into elliptocytic red blood cells with a combined deficiency of protein 4.1, glycophorin C, and p55. *Blood* **87**, 3462-3469 (1996).

18 Cortes, A., Benet, A., Cooke, B. M., Barnwell, J. W. & Reeder, J. C. Ability of Plasmodium falciparum to invade Southeast Asian ovalocytes varies between parasite lines. *Blood* **104**, 2961-2966, doi:10.1182/blood-2004-06-2136 2004-06-2136 [pii] (2004).

19 Dua, M., Raphael, P., Sijwali, P. S., Rosenthal, P. J. & Hanspal, M. Recombinant falcipain-2 cleaves erythrocyte membrane ankyrin and protein 4.1. *Mol Biochem Parasitol* **116**, 95-99 (2001).

20 Nicolas, V. *et al.* Rh-RhAG/Ankyrin-R, a New Interaction Site between the Membrane Bilayer and the Red Cell Skeleton, Is Impaired by Rhnull-associated Mutation. *Journal of Biological Chemistry* **278**, 25526-25533, doi:10.1074/jbc.M302816200 (2003).

21 Grey, J. L., Kodippili, G. C., Simon, K. & Low, P. S. Identification of contact sites between ankyrin and band 3 in the human erythrocyte membrane. *Biochemistry* **51**, 6838-6846, doi:10.1021/bi300693k (2012).

22 Su, Y. *et al.* Associations of protein 4.2 with band 3 and ankyrin. *Molecular and cellular biochemistry* **289**, 159-166, doi:10.1007/s11010-006-9159-x (2006).

23 Eber, S. W. *et al.* Ankyrin-1 mutations are a major cause of dominant and recessive hereditary spherocytosis. *Nat Genet* **13**, 214-218, doi:10.1038/ng0696-214 (1996).

24 Casale, M. & Perrotta, S. Splenectomy for hereditary spherocytosis: complete, partial or not at all? *Expert review of hematology* **4**, 627-635, doi:10.1586/ehm.11.51 (2011).

25 Godal, H. C. & Heisto, H. High prevalence of increased osmotic fragility of red blood cells among Norwegian blood donors. *Scandinavian journal of haematology* **27**, 30-34 (1981).

26 Eber, S. W., Pekrun, A., Neufeldt, A. & Schroter, W. Prevalence of increased osmotic fragility of erythrocytes in German blood donors: screening using a modified glycerol lysis test. *Annals of hematology* **64**, 88-92 (1992).

27 Jensson, O., Jonasson, J. L. & Magnusson, S. Studies on herediatary spherocytosis in Iceland. *Acta medica Scandinavica* **201**, 187-195 (1977).

28 Yawata, Y. *et al.* Characteristic features of the genotype and phenotype of hereditary spherocytosis in the Japanese population. *Int J Hematol* **71**, 118-135 (2000).

29 Glele-Kakai, C. *et al.* Epidemiological studies of spectrin mutations related to hereditary elliptocytosis and spectrin polymorphisms in Benin. *Br J Haematol* **95**, 57-66 (1996).

30 Shear, H. L., Roth, E. F., Jr., Ng, C. & Nagel, R. L. Resistance to malaria in ankyrin and spectrin deficient mice. *Br J Haematol* **78**, 555-560 (1991).

31 Greth, A. *et al.* A novel ENU-mutation in ankyrin-1 disrupts malaria parasite maturation in red blood cells of mice. *PLoS One* **7**, e38999, doi:10.1371/journal.pone.0038999 (2012).

32 Rank, G. *et al.* Novel roles for erythroid Ankyrin-1 revealed through an ENU-induced null mouse mutant. *Blood* **113**, 3352-3362, doi:blood-2008-08-172841 [pii] 10.1182/blood-2008-08-172841 (2009).

33 Stephens, R., Culleton, R. L. & Lamb, T. J. The contribution of *Plasmodium chabaudi* to our understanding of malaria. *Trends in Parasitology* **28**, 73-82, doi:10.1016/j.pt.2011.10.006 (2012).

564 34 Ayi, K., Turrini, F., Piga, A. & Arese, P. Enhanced phagocytosis of ring-parasitized mutant
565 erythrocytes: a common mechanism that may explain protection against falciparum malaria
566 in sickle trait and beta-thalassemia trait. *Blood* **104**, 3364-3371, doi:10.1182/blood-2003-11-
567 3820 (2004).
568 35 McMorran, B. J. *et al.* Platelets Kill Intraerythrocytic Malarial Parasites and Mediate Survival
569 to Infection. *Science* **323**, 797-800, doi:10.1126/science.1166296 (2009).
570 36 Gallagher, P. G. Hematologically important mutations: ankyrin variants in hereditary
571 spherocytosis. *Blood Cells Mol Dis* **35**, 345-347, doi:10.1016/j.bcmd.2005.08.008 (2005).
572 37 Nakanishi, H., Kanzaki, A., Yawata, A., Yamada, O. & Yawata, Y. Ankyrin gene mutations in
573 japanese patients with hereditary spherocytosis. *Int J Hematol* **73**, 54-63 (2001).
574 38 Edelman, E. J., Maksimova, Y., Duru, F., Altay, C. & Gallagher, P. G. A complex splicing defect
575 associated with homozygous ankyrin-deficient hereditary spherocytosis. *Blood* **109**, 5491-
576 5493, doi:10.1182/blood-2006-09-046573 (2007).
577 39 Kyrylkova, K., Kyryachenko, S., Leid, M. & Kioussi, C. Detection of apoptosis by TUNEL assay.
578 *Methods Mol Biol* **887**, 41-47, doi:10.1007/978-1-61779-860-3_5 (2012).
579 40 Straat, M., van Bruggen, R., de Korte, D. & Juffermans, N. P. Red blood cell clearance in
580 inflammation. *Transfusion medicine and hemotherapy : offizielles Organ der Deutschen*
581 *Gesellschaft fur Transfusionsmedizin und Immunhamatologie* **39**, 353-361,
582 doi:10.1159/000342229 (2012).
583 41 Jakeman, G., Saul, A., Hogarth, W. & Collins, W. Anaemia of acute malaria infections in non-
584 immune patients primarily results from destruction of uninfected erythrocytes. *Parasitology*
585 **119**, 127-133 (1999).
586 42 Lamikanra, A. A. *et al.* Malarial anemia: of mice and men. *Blood* **110**, 18-28 (2007).
587 43 Dondorp, A. M. *et al.* Prognostic significance of reduced red blood cell deformability in
588 severe falciparum malaria. *Am J Trop Med Hyg* **57**, 507-511 (1997).
589 44 Dondorp, A. *et al.* The role of reduced red cell deformability in the pathogenesis of severe
590 falciparum malaria and its restoration by blood transfusion. *Transactions of the Royal Society*
591 *of Tropical Medicine and Hygiene* **96**, 282-286 (2002).
592 45 Deplaine, G. *et al.* The sensing of poorly deformable red blood cells by the human spleen can
593 be mimicked in vitro. *Blood* **117**, e88-95, doi:10.1182/blood-2010-10-312801 (2011).
594 46 Hortle, E. *et al.* Adenosine monophosphate deaminase 3 activation shortens erythrocyte
595 half-life and provides malaria resistance in mice. *Blood*, doi:10.1182/blood-2015-09-666834
596 (2016).
597 47 Bauer, D. C., McMorran, B. J., Foote, S. J. & Burgio, G. Genome-wide analysis of chemically
598 induced mutations in mouse in phenotype-driven screens. *BMC Genomics* **16**, 1-8,
599 doi:10.1186/s12864-015-2073-4 (2015).
600 48 Wang, K., Li, M. & Hakonarson, H. ANNOVAR: functional annotation of genetic variants from
601 high-throughput sequencing data. *Nucleic Acids Research* **38**, e164-e164,
602 doi:10.1093/nar/gkq603 (2010).
603 49 Livak, K. J. & Schmittgen, T. D. Analysis of relative gene expression data using real-time
604 quantitative PCR and the 2− ΔΔCT method. *methods* **25**, 402-408 (2001).
605 50 Jarra, W. & Brown, K. Protective immunity to malaria: studies with cloned lines of
606 Plasmodium chabaudi and P. berghei in CBA/Ca mice. I. The effectiveness and inter‐and
607 intra‐species specificity of immunity induced by infection. *Parasite immunology* **7**, 595-606
608 (1985).
609 51 Lelliott, P. M., Lampkin, S., McMorran, B. J., Foote, S. J. & Burgio, G. A flow cytometric assay
610 to quantify invasion of red blood cells by rodent Plasmodium parasites in vivo. *Malar J* **13**,
611 100, doi:10.1186/1475-2875-13-100 (2014).
612 52 Lelliott, P. M., McMorran, B. J., Foote, S. J. & Burgio, G. In vivo assessment of rodent
613 Plasmodium parasitemia and merozoite invasion by flow cytometry. *JoVE (Journal of*
614 *Visualized Experiments)*, e52736-e52736 (2015).

615

616 **Acknowledgement**

617 We would like to acknowledge Shelley Lampkin and Australian Phenomics Facility (APF) for the
618 maintenance of the mouse colonies. This study was funded by the National Health and Medical
619 Research Council of Australia (Program Grant 490037, and Project Grants 605524 and APP1047090),
620 Australian Society of Parasitology (ASP), OzEMalaR, National Collaborative Research Infrastructure
621 Strategy (NCRIS), the Education Investment Fund from the Department of Education and Training,
622 the Australian Phenomics Network, Howard Hughes Medical Institute and the Bill and Melinda Gates
623 Foundation.

624

625

626

627 **Figure Legends**

628 **Figure 1**. **The phenotypic characterisation of *Ank-1*$^{(MRI61689/+)}$ mice.** The morphology of *Ank-1*$^{(MRI61689/+)}$
629 and *Ank-1*$^{(MRI61689/MRI61689)}$ erythrocytes under light microscopy with Giemsa stain (a) and scanning
630 electron microscopy (b). The osmotic fragility curve of wild-type and *Ank-1*$^{(MRI61689/+)}$ erythrocytes
631 when subjected to osmotic stress (c) (n=5-7 per group). The *in-vitro* spleen retention rate of wild-
632 type and *Ank-1*$^{(MRI61689/+)}$ erythrocytes when passing through filter beds (d) (n=3 per group). **
633 indicates P<0.01, *** indicates P<0.001, and all error bars are standard error of mean (SEM).

634

635 **Figure 2**. **The identification of *Ank-1*$^{(MRI61689)}$ mutation and its effects on transcription.** The
636 sequencing of *Ank-1*$^{(MRI61689)}$ mutation, showing a T to A transversion (a). Gel electrophoresis of
637 amplified cDNA product from wild-type, *Ank-1*$^{(MRI61689/+)}$ and *Ank-1*$^{(MRI61689/MRI61689)}$ embryonic livers
638 with primers that spanned the exon 17 to 21 of ankyrin-1 cDNA (primer set 1) (b). The sequencing
639 results of both bands, showing exon skipping in the abnormal transcript of *Ank-1*$^{(MRI61689/MRI61689)}$
640 embryonic liver (c). Gel electrophoresis of amplified cDNA product from wild-type, *Ank-1*$^{(MRI61689/+)}$
641 and *Ank-1*$^{(MRI61689/MRI61689)}$ embryonic livers with primers that contained the predicted 11bp insertion
642 (primer set 2) (d). Sequencing result showing an 11bp insertion between exon 17 and 18 cDNA of the
643 *Ank-1*$^{(MRI61689)}$ transcript (e). The predicted effect of the insertion on the translation of ankyrin-1,
644 showing a frameshift and a premature chain termination (f).

645

646 **Figure 3**. **The effect of *Ank-1*$^{(MRI61689)}$ mutation on the *Ank-1* expression.** Quantitative PCR showing
647 the ankyrin-1 mRNA levels in both *Ank-1*$^{(MRI61689/+)}$ and *Ank-1*$^{(MRI61689/MRI61689)}$ embryonic liver (a). The
648 protein levels of various cytoskeletal proteins examined with both Coomassie (b) and Western blot
649 (c). The relative protein levels of ankyrin-1 calculated from the western blot (d) (n=3 per group).
650 Error bars indicate SEM.

651

652 **Figure 4**. **The response of *Ank-1*$^{(MRI61689/+)}$ mice to malaria infection.** The parasite load of wild-type
653 and *Ank-1*$^{(MRI61689/+)}$ mice when infected with 1x10^{4} *P. chabaudi* (a) and the associated survival curve
654 (b). To determine the mechanisms of resistance, parasite intra-erythrocytic growth was assessed
655 through TUNEL assay at 1-10% parasitemia during late trophozoite stage, as visualised from
656 immunofluorescent images showing presence of parasites and TUNEL-positive parasites (c). The
657 number of TUNEL-positive parasites in both wild-type and *Ank-1*$^{(MRI61689/+)}$ mice were counted and
658 expressed as a percentage (d) (n=3). For parasite invasion and RBC clearance, The IVET assay was
659 done showing the ratio of infected *Ank-1*$^{(MRI61689/+)}$ to wild-type erythrocytes over 36 hours (e) and
660 the relative number *Ank-1*$^{(MRI61689/+)}$ and wild-type erythrocyte in both infected and uninfected mice
661 (f) during *P. chabaudi* infection (n=7). ** indicates P<0.01, *** indicates P<0.001, ## and ###
662 indicates P<0.01 and P<0.001 respectively when compared to wild-type RBC number in infected mice,
663 whereas ^^ indicates P<0.01 when compared to *Ank-1*$^{(MRI61689/+)}$ RBC number in uninfected mice.
664 Error bars indicate SEM.

665

666 **Tables**

	WBC ($x10^6$ /ml)	RBC ($x10^9$ /ml)	HGB (g/L)	MCV (fL)	MCH (pg)	MCHC (g/L)	PLT ($x10^6$ /ml)	%Retics
Wild type	8.7±0.5	10.5±0.1	153.2±2.2	51.4±0.4	14.6±0.1	283.6±2.8	1151±57	2.69±0.26
Ank-1$^{(MRI61689/+)}$	11.9±4.5	11.1±0.1	151.2±1.4	46.1±0.2	13.5±0.1	281.4±9.3	1151±61	2.24±0.21
p-values	NS	P<0.01	NS	P<0.001	P<0.001	NS	NS	NS

667

668 **Table 1**. **The complete blood count of *Ank-1*$^{(MRI61689/+)}$ mice.** The haematological parameters of *Ank-*
669 *1*$^{(MRI61689/+)}$ compared to wild-type mice (n=19-25). WBC = white blood cell count; RBC = red blood cell
670 count; HGB = haemoglobin; MCV = mean corpuscular volume; MCH = mean corpuscular
671 haemoglobin; MCHC = mean corpuscular haemoglobin concentration; PLT = platelet
672 concentration; %Retics = percentage of reticulocytes.

673

Chromosome	Gene name	Location	Reference base	Variant base	Number of mutant mice with mutation	LOD score (Threshold: 2.08)
9	Acp5	22129643	C	A	(3/8)	-0.32
8	Kcnk1	126025024	C	T	(4/8)	0
17	Epas1	86825679	A	T	(0/8)	-2.33
7	Picalm	90165538	G	T	(0/8)	-2.33
18	Socs6	88869240	A	G	(5/8)	0.32
8	Ank1	23106019	T	A	(8/8)	2.33

674

675 **Table 2: The identification of MRI61689 mutation.** Six variants were selected from the exome
676 sequencing, each mutation was sequenced in *Ank-1*$^{(MRI61689/+)}$ mice and the number of mutant mice
677 carrying each mutation was determined and LOD score was calculated, with LOD threshold being
678 2.08 (n=8).

679

680

Figure 1

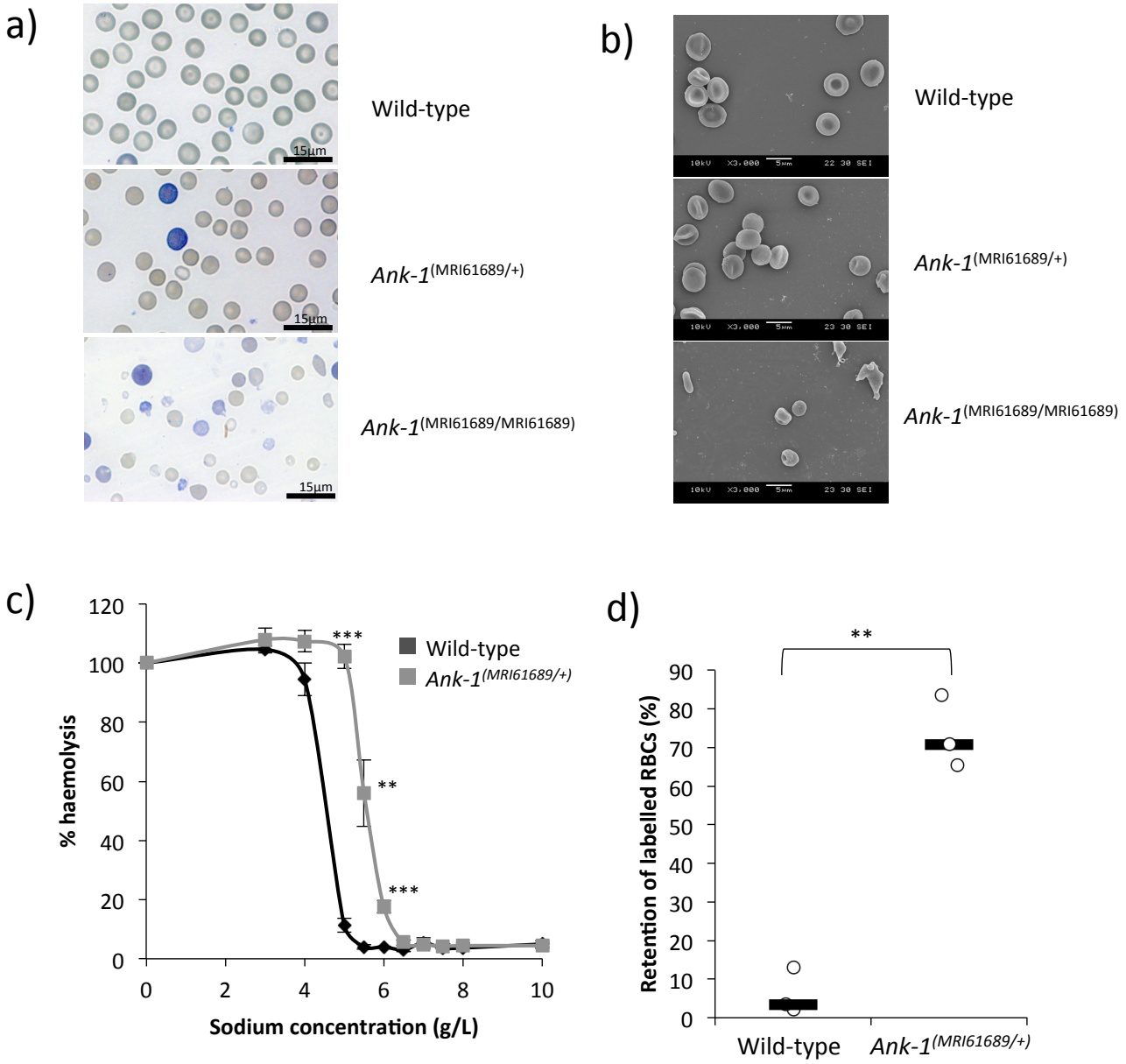
a)
15µm
Wild-type
Ank-1(MRI61689/+)
Ank-1(MRI61689/MRI61689)
b)
Wild-type
Ank-1(MRI61689/+)
Ank-1(MRI61689/MRI61689)
c)
% haemolysis
Sodium concentration (g/L)
Wild-type
Ank-1(MRI61689/+)
***
**
d)
Retention of labelled RBCs (%)
Wild-type
Ank-1(MRI61689/+)
**

Figure 2

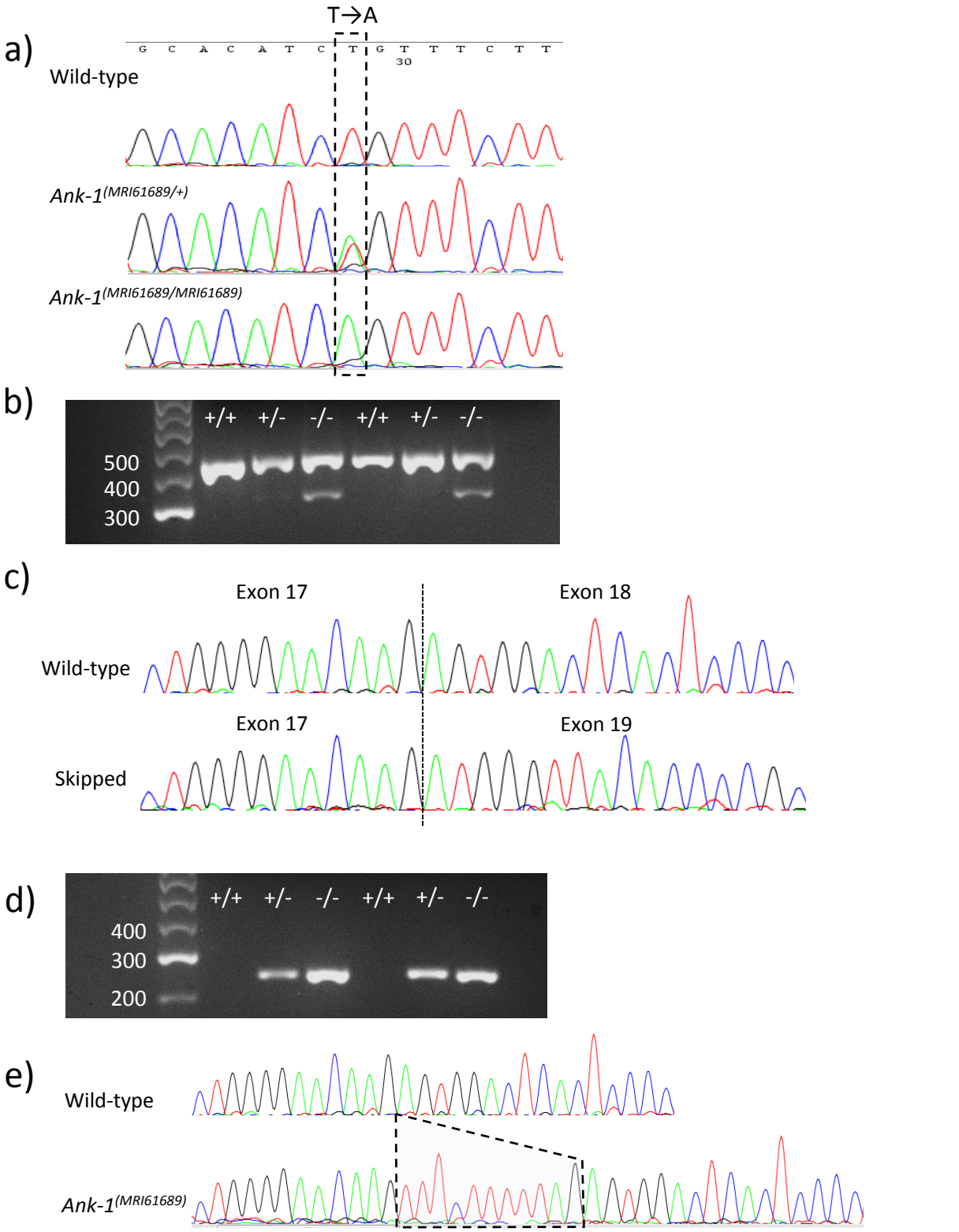

f)

Wild-type gca cat ctg ttt ctt ttt ag AGT GGA CTC ACT CCC
---------- Ser Gly Leu Thr Pro

Ank-1(MRI61689) gca cat cag TTT CTT TTT AGA GTG GAC TCA CTC CC……TGA
---------- Phe Leu Phe Arg Val Asp Ser Leu……STOP

Figure 3

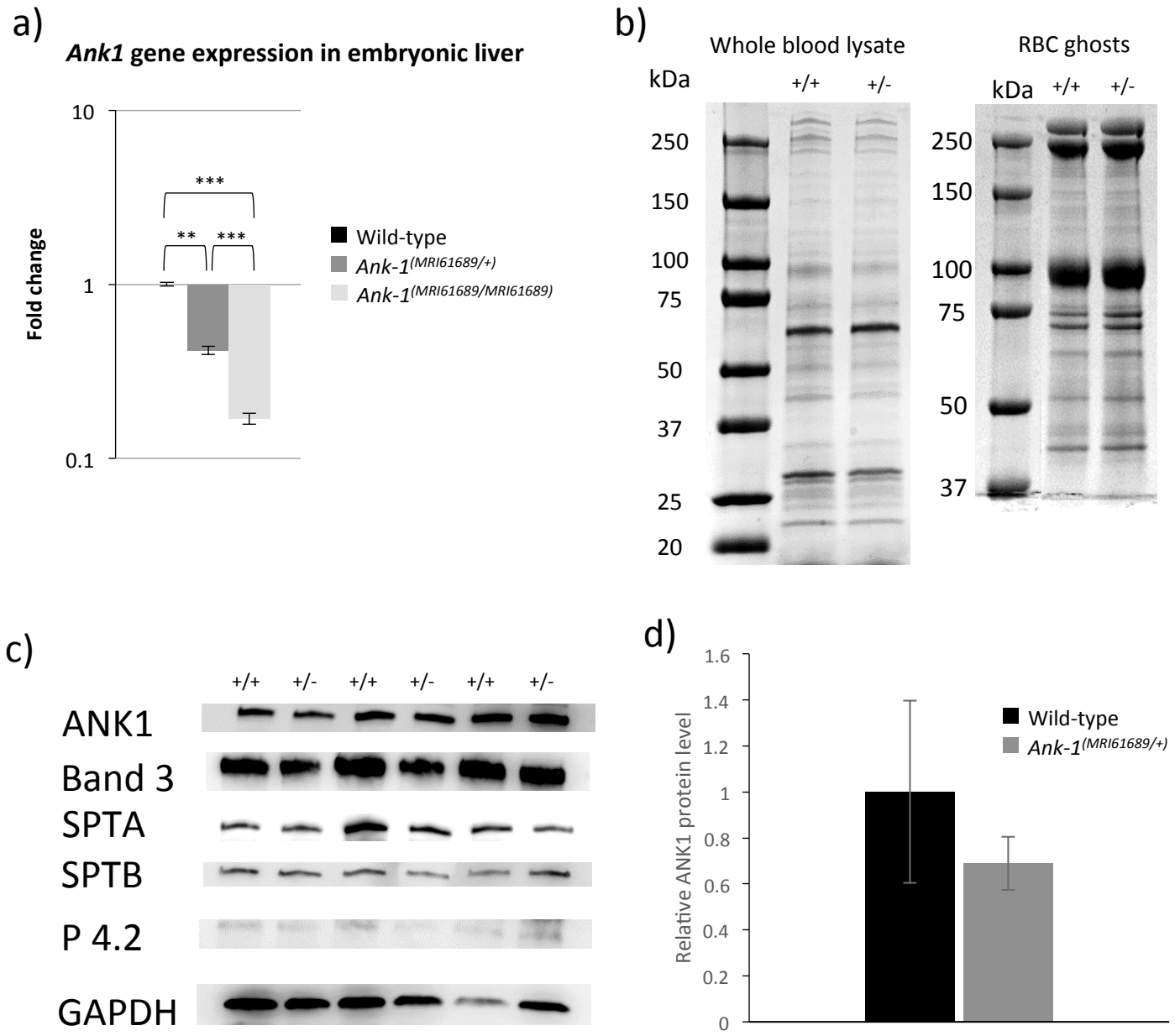
a)
Ank1 gene expression in embryonic liver
Fold change
10
1
0.1
***
**
***
Wild-type
Ank-1(MRI61689/+)
Ank-1(MRI61689/MRI61689)
b)
Whole blood lysate
RBC ghosts
kDa
+/+
+/-
250
150
100
75
50
37
25
20
c)
+/+
+/-
ANK1
Band 3
SPTA
SPTB
P 4.2
GAPDH
d)
Relative ANK1 protein level
1.6
1.4
1.2
1
0.8
0.6
0.4
0.2
0
Wild-type
Ank-1(MRI61689/+)

Figure 4

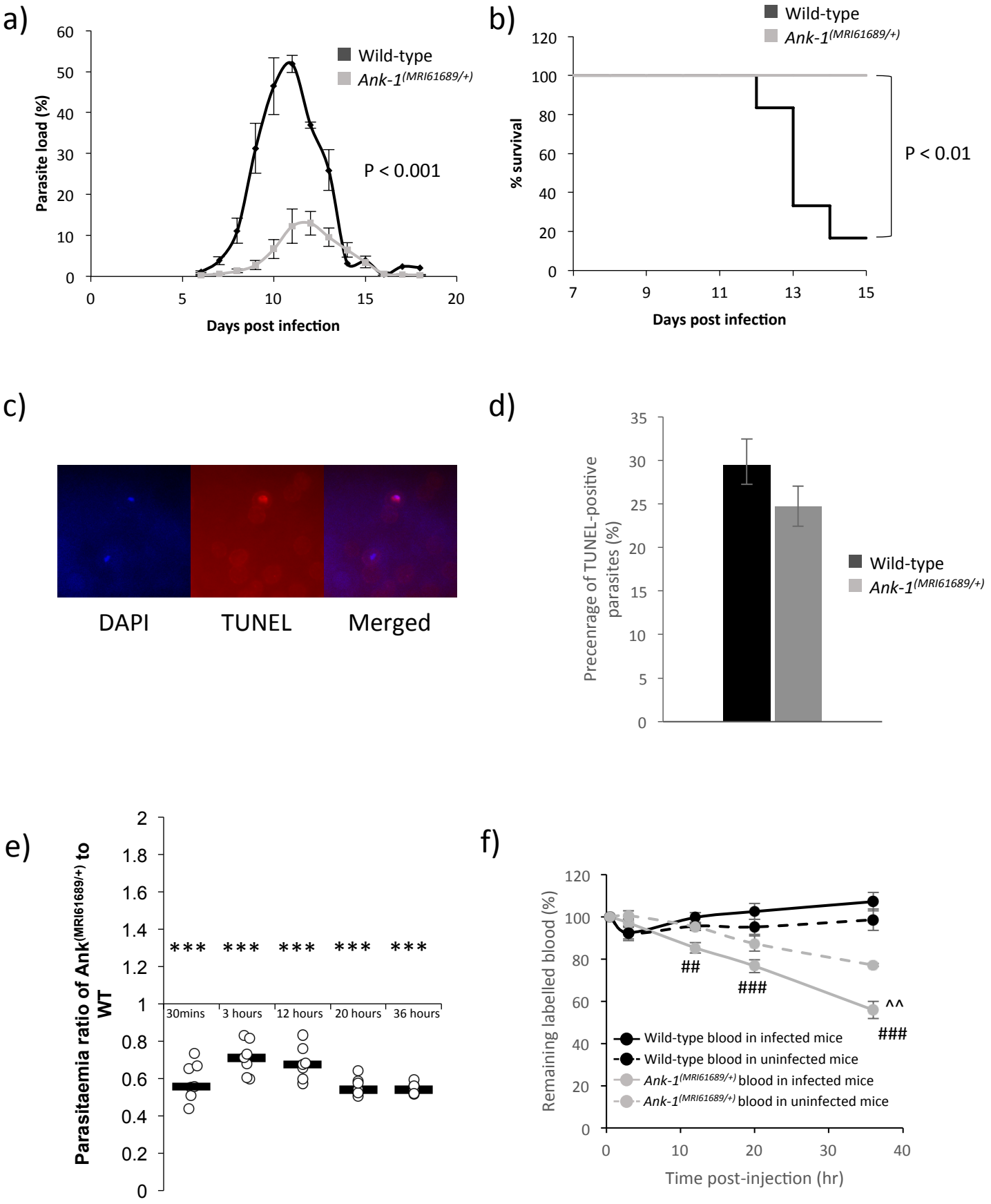
a)
Parasite load (%)
Days post infection
Wild-type
Ank-1(MRI61689/+)
P < 0.001
b)
% survival
Days post infection
Wild-type
Ank-1(MRI61689/+)
P < 0.01
c)
DAPI
TUNEL
Merged
d)
Precenrage of TUNEL-positive parasites (%)
Wild-type
Ank-1(MRI61689/+)
e)
Parasitaemia ratio of Ank(MRI61689/+) to WT
30mins
3 hours
12 hours
20 hours
36 hours
***
f)
Remaining labelled blood (%)
Time post-injection (hr)
Wild-type blood in infected mice
Wild-type blood in uninfected mice
Ank-1(MRI61689/+) blood in infected mice
Ank-1(MRI61689/+) blood in uninfected mice
##
###
^^
###